Two-Photon Lee-Goldburg NMR: Simultaneous Homonuclear Decoupling and Signal Acquisition

Carl A. Michal*, Simon P. Hastings, and Lik Hang Lee
Department of Physics and Astronomy, University of British Columbia, 6224 Agricultural Road, Vancouver, BC, Canada, V6T 1Z1
(Dated: November, 2007)
(The Journal of Chemical Physics **128**, 052301 (2008).)

We present NMR signals from a strongly coupled homonuclear spin system, ^{1}H nuclei in adamantane, acquired with simultaneous two-photon excitation under conditions of the Lee-Goldburg experiment. Small coils, of inside diameter 0.36 mm, are used to achieve two-photon nutation frequencies of $\sim$ 20 kHz. The very large rf field strengths required give rise to large Bloch-Siegert shifts that cannot be neglected. These experiments are found to be extremely sensitive to inhomogeneity of the applied rf field, and due to the Bloch-Siegert shift exhibit a large asymmetry in response between the upper and lower Lee-Goldburg offsets. Two-photon excitation has the potential to enhance both the sensitivity and performance of homonuclear dipolar decoupling, but is made challenging by the high rf power required and the difficulties introduced by the inhomogeneous Bloch-Siegert shift. We briefly discuss a variation of the frequency-switched Lee-Goldburg technique, called four-quadrant Lee-Goldburg (4QLG) that produces net precession in the x-y plane, with a reduced chemical shift scaling factor of 1/3.

Introduction

The acquisition of high-resolution NMR spectra in the solid-state is made difficult by strong internuclear dipolar couplings. Heteronuclear dipolar interactions can be removed by continuous rf irradiation applied to the non-detected nuclei. This is a common situation in organic samples, where one often observes nuclei such as ^{13}C, ^{15}N or ^{31}P in the presence of an abundant ^{1}H reservoir. A variety of irradiation schemes have been developed over the past dozen years to improve the efficiency of such decoupling, examples include two-pulse phase-modulation (TPPM)[1], small phase incremental alteration (SPINAL)[2], XiX[3], and symmetry based adiabatic rf schemes[4,5].

The acquisition of high-resolution spectra in the presence of strong homonuclear dipolar couplings, as often exist between abundant ^{1}H spins, is more challenging due to the strength and symmetry of the ^{1}H-^{1}H homonuclear couplings. A number of rf irradiation schemes have been developed for this situation, but the design of such sequences is more complicated, as the goal is to eliminate the homonuclear dipolar Hamiltonian while simultaneously maximizing the scaling factor of the chemical shift Hamiltonian. Many such methods are based upon Lee and Goldburg's off-resonance irradiation scheme[6], where an effective field at the magic angle in the rotating frame makes the time-averaged homonuclear dipolar Hamiltonian vanish, leaving a chemical shift Hamiltonian scaled by $1/\sqrt{3}$. This effect has formed the basis of a number of homonuclear decoupling sequences. To actually acquire ^{1}H spectra with these types of sequences, decays must be acquired point-by-point in a two-dimensional fashion, or the sequences must be modified to incorporate an rf-free window during which the signal is observed, as has been done with the frequency-switched Lee-Goldburg (FSLG)[7] and phase-modulated Lee-Goldburg (PMLG)[8] sequences. In contrast to the continuous irradiation of the Lee-Goldburg based methods, a second approach has been to use cycles composed of short rf pulses to create a time-averaged Hamiltonian in which the homonuclear dipolar interaction is absent. A great number of such sequences have been developed, among the best known of these are WAHUHA[9,10], MREV[11,12], BR24[13] and Cory's 24 pulse scheme[14]. A third successful approach has been to numerically[15] or experimentally[16] optimize the time-dependent phase of a continuous rf field. Again these sequences have used windows in the rf[16,17] to allow signal detection. In all of these cases, the desired signal can only be detected when the rf excitation is turned off. This restricts the sensitivity of the experiment, as the receiver is generally only turned on for a very small fraction of the total acquisition time. In addition, the performance of the sequence may be negatively impacted by the reduction in duty-cycle required for the detection windows, and also by the rf transients introduced by the rf turn-off and turn-on at the beginning and end of the detection windows.

Two-photon excitation has recently been shown to be a feasible tool for manipulating nuclear spins while simultaneously acquiring NMR signals from them[18,19]. A major challenge to applying two-photon excitation generally is the very small effective excitation field that is achieved with moderate rf power due to the B_1^2/B_0 scaling of the effective field. This excitation efficiency has been increased somewhat by the use of two-colour excitation[19], where two different frequency rf fields, having frequencies that sum to or differ by the resonance frequency, are simultaneously applied, at the expense of additional

*To whom correspondence should be addressed.
Email: michal@physics.ubc.ca. Fax: (604) 822-5324

hardware complexity.

In this work, we demonstrate two-photon homonuclear decoupling with simultaneous acquisition of ^{1}H NMR signals. This technique has the potential to allow acquisition of high-resolution ^{1}H NMR spectra without the sensitivity trade-off required by windowed acquisition. In principle, maximal sensitivity can be achieved because the receiver is turned on at all times, and the cycle-time of the decoupling can be made as short as possible with the given rf power available, because the rf excitation is also turned on at all times. This strategy is demonstrated using Lee-Goldburg irradiation of an adamantane sample in a micro-coil, in which the very large rf field strength allows two-photon effective fields of useful amplitude.

Theory

Lee Goldburg Irradiation

Lee and Goldburg[6] devised a method by which homonuclear dipolar interactions could be efficiently decoupled, while chemical shifts and heteronuclear couplings remain. When an rf field is applied off-resonance, a transformation into a frame aligned so that its z axis points along the effective field in the rotating frame, at an angle θ to the static B_0, shows immediately that the secular part of the homonuclear dipolar Hamiltonian is scaled by a factor of $(3\cos^2\theta - 1)/2$, while the heteronuclear dipolar and chemical shift Hamiltonians are scaled by $\cos\theta$. If the resonance offset is chosen so that $\theta = \mathrm{acos}(1/\sqrt{3}) \approx 54.74°$, the secular part of the homonuclear dipolar Hamiltonian vanishes, while the chemical shifts and heteronuclear dipolar couplings are reduced by a factor of $1/\sqrt{3}$. Mehring and Waugh[7] showed that by reversing the direction of the effective field following each 2π rotation around it, the first order correction term to the average homonuclear dipolar Hamiltonian may be canceled, dramatically improving the performance of the sequence. Mehring and Waugh initially carried this out by applying their rf field at the resonance frequency of the sample, and then shifting the main field either up or down in synchrony with 180° rf phase shifts to satisfy the magic angle condition. A similar effect can be achieved by switching the frequency of the irradiation from above the resonance to below with a simultaneous reversal in the rf phase. This technique, shown in Fig. 1a, is known as frequency-switched Lee-Goldburg (FSLG)[20] irradiation. In practice this is often most easily implemented by modulating the phase of a fixed-frequency rf signal. When the cycle time becomes short, hardware limitations can restrict the number of phase increments used in each cycle and it is perhaps not obvious that approximating a smoothly varying phase ramp by a small number of discrete phase steps is reasonable. Vinogradov *et al.*[21,22] have done detailed calculations and experiments in this regime to show that homonuclear decoupling can still be achieved. This manner of implementation of FSLG is known as phase-modulated Lee-Goldburg (PMLG).

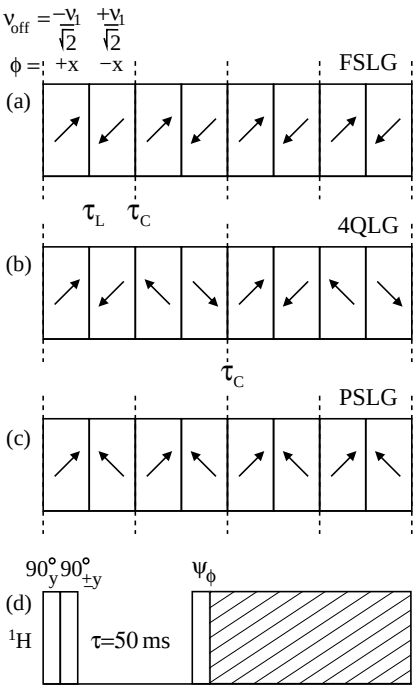

FIG. 1: 1: Pulse sequences. The arrows indicate the direction of the effective field in the rotating frame. A traditional frequency switched Lee-Goldburg sequence is shown in (a). (b) is a modified sequence formed by concatenating two FSLG cycles and reversing the rf phase in the latter half. In (c), the rf is applied at a single resonance offset. The sequences of (b) and (c) result in a net precession about the z axis with a scaling factor of 1/3. τ_L is the time taken for one full rotation about the effective field, given by $\sqrt{2/3}/\nu_1$. τ_C is the duration of a complete cycle, and is $2\tau_L$ in (a) and (c) or $4\tau_L$ in (b). (d) shows the pulse sequence strategy used for averaging of the rf feedthrough in the two-photon NMR experiments. The shaded region represents simultaneous signal acquisition and excitation, with either simple continuous irradiation, or with one of the LG sequences shown. (d) includes an optional tipping pulse of duration ψ and phase ϕ, to prepare the magnetization along the x axis ($\psi = 90°, \phi = -y$), the y axis ($\psi = 90°, \phi = x$), or along the effective field ($\psi = 54.7°, \phi = -y$). The rf frequency offsets shown in this figure (ν_{off}) are measured from the rf-on (*i.e.* Bloch-Siegert shifted) resonant frequency.

These Lee-Goldburg based sequences share the property that the net precession due to the chemical shift is about an axis that forms an angle θ with the static field axis, complicating any spectrum that might be simultaneously acquired. Recently, Bosman *et al.*[23] have shown that imperfections in the rf pulses can be exploited to produce a net precession about the static field axis, while maintaining a relatively large chemical shift scaling factor.

Another way to produce a net precession about the z-axis is to interleave these flip-flop Lee-Goldburg cycles with identical but phase reversed cycles as shown

in Fig. 1b. This sequence, in the absence of rf imperfections, results in a net precession around the z axis with a scaling factor of 1/3, and maintains the cancellation of the first order correction term to the average Hamiltonian. We refer to this sequence as four-quadrant Lee-Goldburg (4QLG) irradiation, because the effective field spends equal times in each of the four quadrants of the x-z plane in the rotating frame. In some of the experiments discussed below, it is advantageous to restrict the rf to only the upper or lower frequency side of resonance, and a sequence such as that shown in Fig. 1c is used, where the effective field is switched between magic angle conditions, but only by switching the rf phase by 180°. In this case, the sequence lacks the requisite symmetry to completely cancel the first order correction to the average Hamiltonian. While we have not evaluated this correction in detail, there does appear to be at least a partial cancellation of the first order correction (it appears that 48 of 80 possible contributing terms cancel). This latter sequence also results in a net precession about the z axis, with a scaling factor of 1/3. We refer to this sequence as phase-switched Lee-Goldburg (PSLG).

Two Photon Excitation

It has been known for years that NMR signals may be excited with rf excitation at frequencies not near to the resonance frequency. In his well-known book, Abragam explains three-photon excitation with a classical vector description[24]. More recently, two-photon excitation has been shown to be a practical technique for exciting NMR signals[18,19], and has the advantage over on-resonance excitation of allowing simultaneous acquisition and excitation. Multi-photon excitation may be performed with a single rf excitation frequency at a sub-multiple of the resonance frequency, or with multiple rf frequencies that sum to or differ by the resonance frequency. Here we confine our discussion to the case of two-photon excitation using rf fields at one-half the normal resonance frequency. The effective field produced by the half-resonance rf in this case can be found easily by transforming into a "phase-modulated rotating frame,"[18] and is given by

$$\nu_1 = \frac{1}{2\pi}\frac{(\gamma\tilde{B}_1)^2 \sin\alpha\cos\alpha}{2\gamma B_0}, \qquad (1)$$

in which α is the angle made by the rf coil and the static magnetic field B_0, γ is the gyromagnetic ratio, and $\tilde{B}_1$ is the amplitude of the linearly oscillating rf. We will refer to the amplitude of the physical rf field applied at the half-resonance frequency by the symbol $\tilde{B}_1$, to emphasize that $\nu_1 \neq \gamma\tilde{B}_1/2\pi$. If the coil was aligned so that it was perpendicular to the z axis and the static magnetic field B_0 reduced to half its value, the nutation frequency (in Hz) would be given by $\gamma\tilde{B}_1/4\pi$. From Eq. 1 it is clear that no two photon excitation will occur if the rf field lies either parallel or perpendicular to the static field axis. This may be understood in terms of the conservation of angular momentum; two rf photons involved in the transition of a nuclear spin between states having angular momentum projection difference $\Delta m = \pm 1$ cannot both carry angular momentum. Hence rf fields both parallel and perpendicular to the static field are required.

The application of any far-off-resonant rf field (one where the strength B_1 and angular frequency ω satisfy $\gamma B_1 \ll |\omega - \gamma B_0|$) leads to a shift in the resonance frequency known as the Bloch-Siegert shift[25]. Because a linearly oscillating resonant field may be decomposed into one rotating resonant component and a second counter-rotating component that is off resonance by $2\gamma B_0$, a linear, resonant field leads to a Bloch-Siegert shift as well. These shifts are small enough to be ignored in many NMR experiments, but in two-photon excitation they are always significant. With our single-coil, half-resonant excitation arrangement, the Bloch Siegert shift, when expressed as $\Delta_{\rm BS} = \nu_{\rm BS}/\nu_0$, the fractional shift in resonant frequency, is given by

$$\Delta_{\rm BS} = \frac{1}{3}\left(\frac{\tilde{B}_1 \sin\alpha}{B_0}\right)^2. \qquad (2)$$

The ratio of the Bloch-Siegert shift to the nutation frequency provided by the rf is

$$\frac{\nu_{\rm BS}}{\nu_1} = \frac{2}{3}\tan\alpha. \qquad (3)$$

If the coil is oriented for maximum excitation efficiency ($\alpha = 45°$), then $\tan\alpha = 1$, and the ratio becomes simply 2/3.

Experiment

Experiments were performed using a home-built NMR spectrometer, having fast small-angle phase-shifting capability. The rf transmitters employ AD9854 digital synthesizers (Analog Devices, Norwood, MA), having phase shifting resolution of 0.02°. The spectrometer includes a fully digital receiver, similar to one described previously[26]. These devices are controlled by two PulseBlaster PB-24 pulse programmer boards (SpinCore Technologies, Gainesville, FL). A 4.7 T superconducting magnet (Oxford Instruments, Oxford, UK) was chosen over higher field strengths to increase the two-photon effective field. A coil was constructed from 5 turns of 40 gauge wire wound around a short section of polyimide-coated glass capillary, having an outside diameter of 358 μm and an inside diameter of 248 μm. (Polymicro Technologies, Phoenix, AZ). Small grains of adamantane (Fluka-Chemie, Buchs, Switzerland) were packed into the capillary by hand under a microscope, and the capillary then sealed with a two-part epoxy (Devcon, Danvers, MA). The coil was mounted in a home-built doubly resonant (100 and 200 MHz) probe so that the coil axis made an angle of $\sim 45°$ with the main field axis.

500 W of rf excitation at 100 MHz produced by a Kalmus model LP1000 (Kalmus Engineering, Woodinville, WA) amplifier led to two-photon nutation frequencies of $\sim$ 20 kHz. If the coil was oriented with its axis perpendicular to B_0 and the main field lowered from 4.7 to 2.35 T, this rf would produce an on-resonance nutation frequency of approximately 2 MHz, corresponding to a 90° pulse width of 0.125 μs.

Significant care was required in the set-up of the signal paths between the rf power amplifier, the probe, and the pre-amplifier. Selective 200 MHz band-pass filters were employed on the receive side of the probe to eliminate any 100 MHz rf leakage through the probe. During excitation a small amount of 200 MHz rf is generated due to nonlinearities in the materials of the probe, cables, connectors, and filters. This 200 MHz signal is very small, but does appear at essentially the same frequency as the NMR signal of interest. For this reason, our experiments are phase-cycled in a way to allow the subtraction of the near-resonance rf leakage. All experiments were performed with the sequence shown in Fig. 1d, which consists of a pair of 90° pulses with either identical phases, or a 90° phase shift (which produces a 180° shift in the rotating frame at the resonance frequency) to alternately prepare the magnetization along $-\hat{z}$ or $+\hat{z}$. The receiver was cycled by 180° on alternate scans to enable the co-addition of the true NMR signals. These pre-pulses were followed by a 50 ms delay to allow any remaining in-plane magnetization to decay before the decoupling sequence began. We found that even minor adjustments to any of the connections could cause relatively large changes in the amount and stability of the 200 MHz parasitic rf.

Because the Bloch-Siegert shift is always significant with two-photon excitation, tuning up the spectrometer for Lee-Goldburg excitation is less straightforward than in the usual near-resonance case. The problem is that usually one knows the resonance frequency of the nuclear spins to high precision, and only the rf field strength needs to be measured. But in our case, since the frequency is shifted during irradiation by the Bloch-Siegert shift, one initially knows neither the strength of the rf field nor the resonance frequency during irradiation. The two values are connected by Eq. 3, but unfortunately, unless the orientation of the coil (*i.e.* the angle α) is known to very high precision, both values must be determined. Simply setting the transmitter and receiver frequencies (set to differ by exactly a factor of two) so that the received NMR signals are on resonance produces a nutation plot with large pulse-width dependent phase shifts, as found when the NMR signal is off resonance by a frequency similar to ν_1. For calibration here, we simply turn the rf transmitter and receiver on simultaneously, and measure nutation curves for various values of the frequency offset. A maximum in the nutation period is observed at the correct Bloch-Siegert shift, thus providing both the magnitude of the shift as well as the strength of the rf field.

Unless otherwise noted, each data set shown is the result of the co-addition of 1000 scans, acquired with a receiver spectral-width of 500 kHz. Each data set has been subsequently low-pass filtered at 100 kHz and phase corrected.

Results and Discussion

The NMR signals received during continuous excitation for various rf frequency offsets ($\Delta\nu$) are displayed in Fig. 2. In each case the sequence of Fig. 1d was used, with the transmitter frequency set to approximately compensate for the Bloch-Siegert shift during the initial pair of 90° pulses, and then shifted to the desired offset frequency shown. The magnetization is observed to nutate around the effective field in the rotating frame. A decay is observed in the amplitude of the nutation signal, and a portion of the magnetization becomes spin-locked along the rf. When the rf is turned off at the 500 μs mark, a free-induction decay is observed. The first 400 μs of the y-component of each nutation plot has been fitted to a function of the form:

$$S(t) = S_0 \cos(2\pi t/T + \phi) \exp(-t/\tau) + c, \qquad (4)$$

in which S_0 represents the amplitude of the oscillatory signal, T is the period of the oscillation, ϕ is a phase offset, τ is a decay constant, and c is a constant offset. The period of oscillation as a function of transmitter offset frequency is shown in Fig. 3a, where a maximum is clearly seen at an offset $\sim$14 kHz. A fit of these data to a function of the form

$$T(\Delta\nu) = \frac{1}{\sqrt{\nu_1^2 + (\nu_{\rm BS} - \Delta\nu)^2}}, \qquad (5)$$

yields a best fit of $\nu_{\rm BS} = 14.4$ kHz and $\nu_1 = 20.7$ kHz. The ratio of these two: $\nu_{\rm BS}/\nu_1 = 0.695$ is in relatively good agreement with the value of 2/3 expected from Eq. 3. This value is only expected if the coil is aligned at exactly 45° from the static field axis. A value of $\alpha = 46.2°$ would yield the observed $\nu_{\rm BS}/\nu_1$ ratio. This degree of misalignment is certainly possible as the coils are quite tiny and aligned by eye only.

The nutation amplitude decay constant, τ, is shown as a function of $\Delta\nu$ in Fig. 3b. An asymmetric pattern with a broad maximum at $\Delta\nu \sim 30$ kHz is observed. The position of this maximum corresponds roughly to the upper Lee-Goldburg offset (14.4 kHz + 20.7 kHz/$\sqrt{2}$ = 29.0 kHz), but only a hint of a maximum can be observed on the lower frequency side. The dramatic asymmetry in the decay constant between upper and lower offsets is understood upon consideration of the effects of $\tilde{B}_1$ inhomogeneity. Two-photon excitation is more sensitive to rf homogeneity than on-resonance excitation because the effective field strength scales according to the *square* of the half-frequency rf amplitude. In addition, the Bloch-Siegert shift is linearly proportional to ν_1, and similar in amplitude. Thus the resonant frequency as well as ν_1 vary

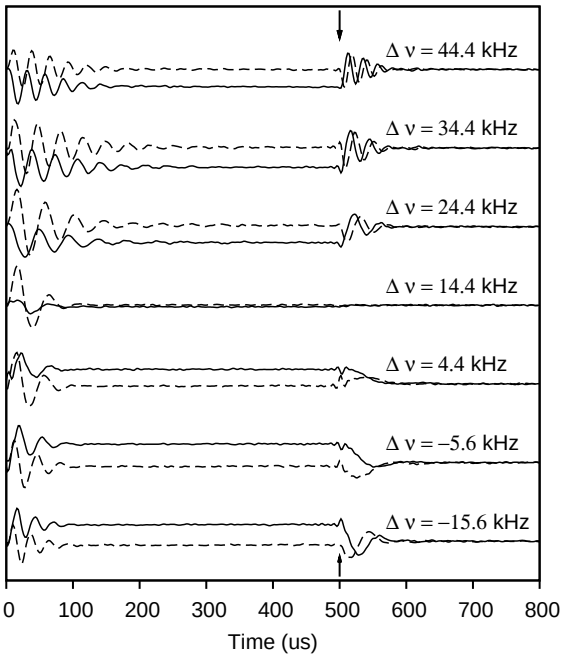

FIG. 2: NMR signals acquired from an adamantane sample under continuous rf irradiation at the offset frequencies shown. The receiver reference was set at exactly twice the transmitter frequency in each case, and offset frequencies correspond to offsets of the receiver reference. Offsets are measured so that a short pulse at an offset of zero produces an NMR signal centered at the receiver reference. Each trace is the result of 400 scans. The arrows indicate the point at 500 μs where the transmitter was shut off. The solid and dashed lines correspond to the x and y components of the magnetization respectively.

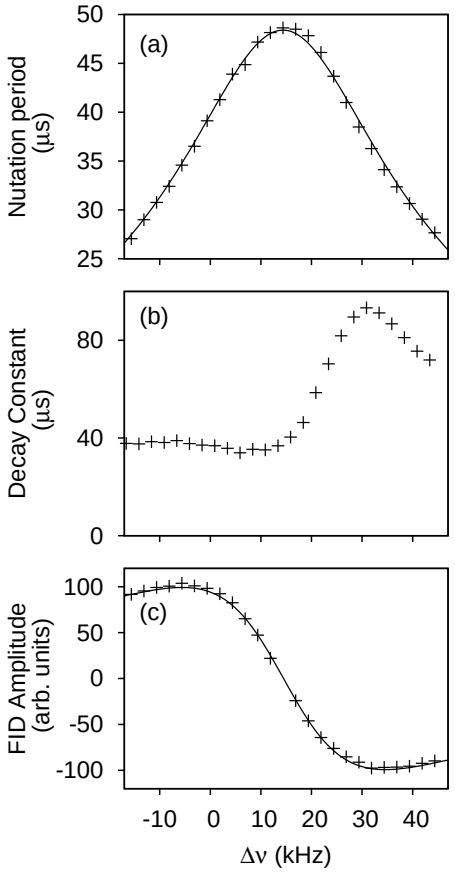

FIG. 3: Calibration of rf field strength and Bloch-Siegert shift. (a) shows the period of nutation observed as a function of transmitter offset, (b) is the decay constant of the nutation, and (c) is the amplitude of the signal that remains following turn-off of the irradiation. The solid lines are fits to equations describing the expected behaviour as explained in the text. The asymmetry of the decay constant at the two Lee-Goldburg offsets is due to rf inhomogeneity.

over the active volume of the coil. Locations in the coil having $\tilde{B}_1$ below the average value have both a smaller $\nu_{\rm BS}$ and ν_1. At the upper Lee-Goldburg offset, a reduced $\nu_{\rm BS}$ and ν_1 means that the transmitter frequency is too high for the Lee-Goldburg offset, so the angle between the effective field and the static field axis is reduced, as illustrated in the upper row of Fig. 4. The amplitude of the effective field is relatively insensitive to this variation though, because the reduction in ν_1 is partially offset by the increased z component of the effective field.

On the lower frequency side however (middle row of Fig. 4), it happens that the Bloch-Siegert shift is almost exactly equal to the Lee-Goldburg offset (for a coil oriented near 45°) and the orientation of the effective field is very insensitive to the $\tilde{B}_1$ inhomogeneity. The amplitude of the effective field however, is very sensitive. The dependencies of the effective field orientation and amplitude on ν_1 strength are shown in Figs. 4c and 4f.

At the upper offset, nuclei at different positions in the coil experience effective fields pointing in different directions, but having similar amplitudes. Their magnetizations follow slightly different paths in the rotating frame, but rephase along the z axis each nutation period. At the lower offset, the magnetizations all follow the same path very accurately around the effective field at the magic angle, but at widely differing rates, thus explaining the asymmetry in the decay constant seen in Fig. 3b.

In addition to the upper/lower offset asymmetry in τ, the peak near 29 kHz is itself asymmetric. The amplitude compensation effect of the effective field at the upper offset continues to improve as the offset is further increased, reaching an optimum at an offset of $\nu_1(9 + 4\tan^2\alpha)/6\tan\alpha$ ($\sim$ 45 kHz here). This fact, in combination with the homonuclear decoupling effects of the Lee-Goldburg irradiation, is likely responsible for this asymmetry. The detailed characteristics of both of these asymmetries will depend on the orientation of the coil in the magnetic field (*i.e.* the angle α) as well as on the details of the $\tilde{B}_1$ homogeneity.

The amplitude of the free-induction decay following the 500 μs irradiation of Fig. 2 is shown versus offset frequency in Fig. 3c. These data have been fitted to a

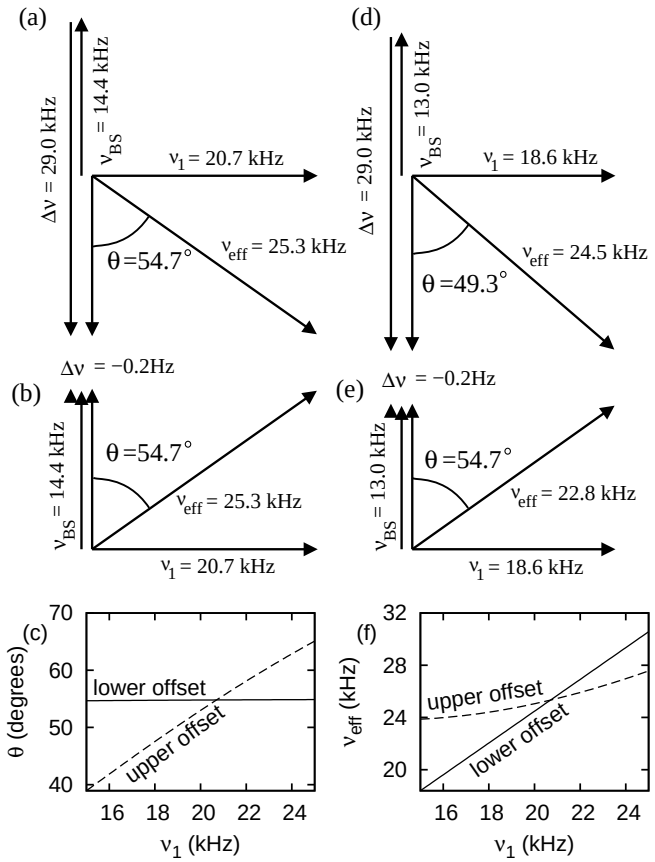

FIG. 4: Illustration of the asymmetric effects of rf inhomogeneity at the upper and lower Lee-Goldburg offsets. At the upper (a) and lower (b) offset frequencies, the z component of the field in the rotating frame may be considered to arise from two pieces. The first is the Bloch-Siegert shift, 14.4 kHz here. The second piece is due to the transmitter offset, $\Delta\nu$, 29.0 kHz at the upper offset and -0.2 kHz at the lower. In (d) and (e), both ν_1 and $\nu_{\rm BS}$ have been reduced by 10% and it is clear that at the lower offset, θ is insensitive to inhomogeneity, but $\nu_{\rm eff}$ is perturbed. At the upper offset θ is significantly altered while $\nu_{\rm eff}$ is only slightly affected. (c) and (f) show the dependence of the θ and $\nu_{\rm eff}$ on ν_1 at the upper and lower Lee-Goldburg offsets, assuming $\nu_{\rm BS} = 2\nu_1 \tan(46.2^\circ)/3$.

function of the form

$$S = S_0 \sin(\theta)\cos(\theta) = S_0 \frac{\nu_1(\nu_{\rm BS} - \Delta\nu)}{\nu_1^2 + (\nu_{\rm BS} - \Delta\nu)^2}, \qquad (6)$$

in which the cos accounts for the projection of the magnetization (initially along z) that ultimately becomes spin-locked along the effective field. The sin accounts for the projection of this spin-locked magnetization into the x-y plane. This function fits the data well, with $\nu_{\rm BS} = 14.3$ kHz and ν_1=20.1 kHz. These values are in good agreement with those found from the fit to the nutation period data in Fig. 3a (of $\nu_{\rm BS} = 14.4$ kHz and ν_1=20.7 kHz), with the differences most likely due to the effects of $\tilde{B}_1$ inhomogeneity.

Next, the receiver and transmitter offsets were increased by 14.4 and 7.2 kHz respectively, and an FSLG sequence was performed with simultaneous signal acquisition. These data are shown in the top row of Fig. 5, plotted versus time and in the x-y plane, along with the expected path of the magnetization. The measured magnetization appears to follow the expected path initially, but after just a couple of nutation periods a fraction becomes spin-locked along the effective field and the nutation about the field rapidly disappears. The failure of this sequence is almost certainly due to $\tilde{B}_1$ inhomogeneity, as the effective field can have different amplitudes and orientations in the two halves of the cycle, dependent upon position inside the coil. In the lower row of Fig. 5, similar signals from the PSLG sequence are shown. This sequence appears to perform relatively well, as here we maintain the rf transmitter always at the positive offset, where the cycle time is relatively insensitive to inhomogeneity. When plotted in the x-y plane, the magnetization is observed to follow a nearly symmetric dumb-bell shaped pattern.

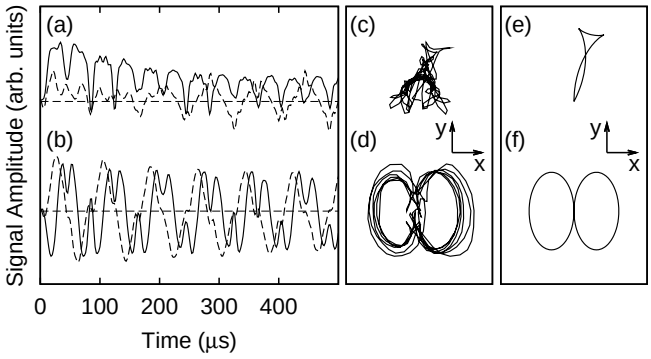

FIG. 5: NMR signals acquired under Lee-Goldburg irradiation. (a) and (c) show signals acquired under traditional FSLG irradiation, while (b) and (d) employ PSLG. In (a) and (b) the x and y components are both plotted as functions of time, while in (c) and (d), the signals are shown in the x-y plane. (e) and (f) show the signals expected for ideal sequences. The frames of observation of the upper and lower rows are different from each other: in the upper row, the transmitter frequency was fixed at the Bloch-Siegert shift and the frequency offset produced by rapid modulation of the phase of the rf transmitter while in the lower row, the transmitter and receiver frequencies were set at the upper Lee-Goldburg condition and the transmitter phase switched by 180° following each 2π nutation.

These latter data may be visualized in three dimensions. Because the magnetization passes through the x-y plane twice per rotation, it is straightforward to fit the envelope of the signals to a decaying function, from which it is possible to infer the z component of the magnetization. The envelope of the data shown in Fig. 5b is well described by a function of the form

$$M(t) = M_1 e^{-t/\tau_1} + M_2 e^{-t/\tau_2}, \qquad (7)$$

and the z component of the magnetization inferred as: $M_z(t) = \pm\sqrt{M(t)^2 - M_x(t)^2 - M_y(t)^2}$, where $M_x(t)$ and

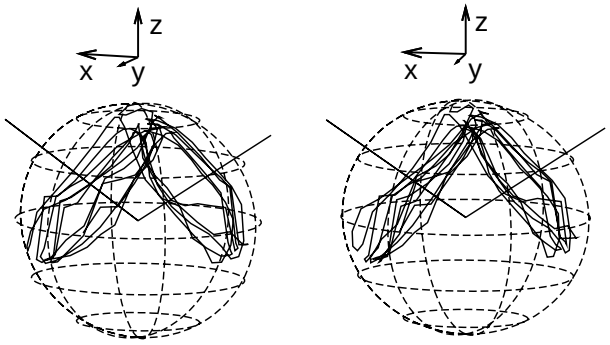

FIG. 6: Stereoscopic view of the path followed by the net nuclear magnetization in three dimensions under the PSLG sequence. The x and y components are the directly measured values shown in Figs. 5b and 5d, while the z component is derived from a fit to the envelope of the x and y components, as described in the text. The straight lines make an angle of 54.74° with the vertical. The first complete cycle has been omitted for clairity.

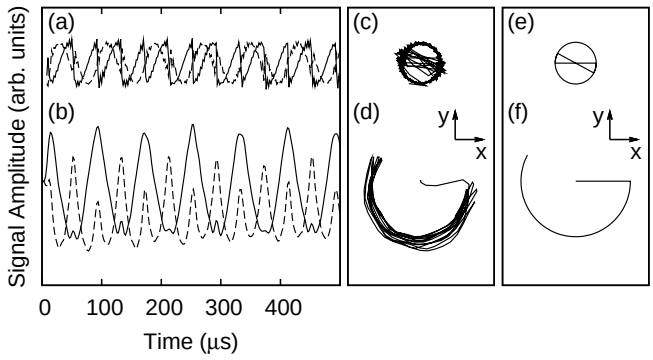

FIG. 7: Spin-locked Lee-Goldburg NMR signals. (a) shows the x and y components of the signals received in a single scan of the FSLG experiment. The observed signal is almost entirely due to feed-through of the transmitter signal. (b) shows signals from the same experiment, following co-addition of 1000 acquisitions. (c) and (d) are the same signals as those in (a) and (b), plotted in the x-y plane. Data in (b) and (d) are increased in scale by a factor of 100, after normalizing by the number of scans, compared to (a) and (c). (e) and (f) show the expected signals for comparison to (c) and (d).

$M_y(t)$ are the measured x and y components. Negative values of the z component are assumed between the two nearby maxima of the in-plane component in each cycle. $M_x(t), M_y(t)$, and $M_z(t)$ are plotted on a sphere in Fig. 6 in a stereoscopic image, allowing direct visualization of the path of the magnetization.

In Fig. 7, signals are shown using the FSLG sequence with the initial magnetization tipped to lie along the effective field in the rotating frame. Along with the NMR signals is a trace showing the feed-through of the rf excitation observed in a single scan. The NMR signals are a factor of ~ 40 smaller than the single-scan feed-through. When these signals are plotted in the x-y plane (Figs. 7c and 7d) it becomes immediately clear that the signal averaging technique employed is effective in eliminating the rf feed-through. In this case the $\tilde{B}_1$ inhomogeneity does not appear to produce the catastrophic effects observed when the magnetization begins along the z axis. These data were acquired in the same way as in the upper trace of Fig. 5 where the transmitter was fixed at the Bloch-Siegert shift frequency, and then phase modulated to produce the off-resonance shifts. The receiver was turned on during the initial 54.7°_{-y} pulse, and this tip of the magnetization is obvious when the data are plotted in the x-y plane.

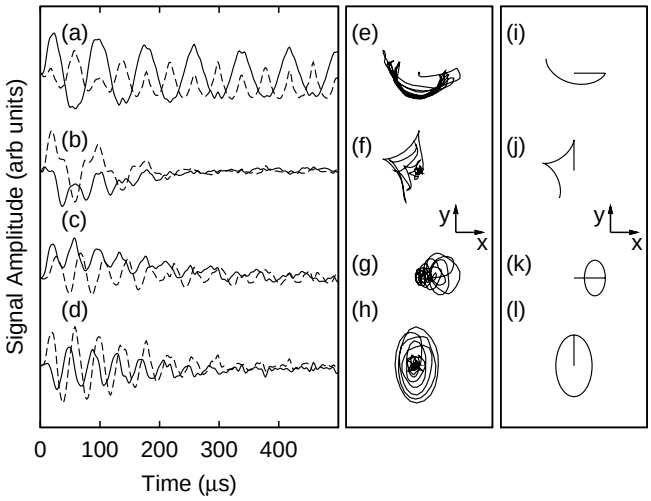

FIG. 8: Lee-Goldburg NMR signals with magnetization prepared in the x-y plane. Signals in (a) and (b) were acquired using the FSLG sequence with the magnetization placed on the x and y axes respectively. (c) and (d) are the same as (a) and (b), but used the PSLG sequence of Fig. 1c. (d)-(h) are the same data as (a)-(d), but plotted in the x-y plane. (i)-(l) show the paths in the x-y plane the magnetization is expected to follow.

The evolution observed when the magnetization is initially placed in the x-y plane, for both the FSLG sequence and the PSLG sequence, is shown in Fig. 8. A large fraction of the magnetization prepared along the x axis rapidly becomes spin-locked under the FSLG sequence, in a similar fashion to that observed with the z starting point in Fig. 5a. The y magnetization clearly follows the correct path, but rapidly decays away, again most likely due to $\tilde{B}_1$ inhomogeneity. With the PSLG sequence, the magnetization follows the expected trajectory for much longer from both starting points. It is clear however, that these sequences do not maintain the magnetization in the x-y plane for nearly long enough to allow the collection of spectra that might be thought of as high-resolution. The 4QLG sequence of Fig. 1b produces the expected trajectories (the expected paths are identical to those of the FSLG sequence in Figs. 8i and 8j for magnetization starting along x or y; when begun along z, the expected path is identical to that in Fig. 5e but with a second branch rotated 180° from the single branch shown), but the signals decay with time constants more similar to those observed

with the PSLG sequence. The decay rates of the magnetization of these sequences depend not only on the performance of the sequence itself, presumably through the first order correction term to the average Hamiltonian, but also on the detailed inhomogeneity of $\tilde{B}_1$.

It is clear from the data shown above that two-photon Lee-Goldburg NMR is possible, but made challenging by the effects of rf inhomogeneity. It is likely that decoupling sequences can be found, perhaps through an optimization procedure as was used in the development of eDUMBO[16], that will be much less sensitive to these effects. Unfortunately, the variations in Bloch-Siegert shift that accompany rf inhomogeneity will likely limit the achievable resolution even so. In this work we have not made serious efforts to optimize the homogeneity; winding the coil with flat wires and restricting the sample to its center area are two straightforward changes that would likely make a marked improvement.

The 4QLG sequence may find application with ordinary near-resonance excitation, as it does provide chemical shift evolution about the z axis, although with a reduced scaling factor. We have not yet investigated the performance of this sequence in any detail.

Conclusions

We have presented NMR signals clearly showing the behaviour expected under rotating-frame magic-angle rf irradiation. Inhomogeneity of the applied rf field has been shown to be very important, due to the fact that both the effective rf field, as well as the resonance frequency (via the Bloch-Siegert shift) depend on the square of the amplitude of the half-resonant rf field applied. While it is clear that two-photon Lee-Goldburg decoupling is likely to remain a curiosity for some time, and is not currently suitable for everyday use in the collection of high-resolution spectra of strongly coupled spin systems, it is possible that further developments in instrumentation and pulse sequences will allow two-photon excitation to become a useful technique in the spectroscopist's toolbox.

We have demonstrated two-photon nutation frequencies of > 20 kHz, representing a dramatic increase over earlier results of ~ 2 kHz[19] and ~ 100 Hz[18]. It is likely that further efforts will produce additional increases in two-photon nutation rates.

A new variation of the FSLG sequence, 4QLG, has been introduced. Because it produces a net evolution of the chemical shift about the z axis, this sequence may provide advantages over other homonuclear decoupling sequences.

Acknowledgments

This work was supported by a grant from the Natural Sciences and Engineering Research Council of Canada.

[1] A. E. Bennett, C. M. Rienstra, M. Auger, K. V. Lakshmi, and R. G. Griffin, J Chem Phys **103**, 6951 (1995).
[2] G. de Paëpe, A. Lesage, and L. Emsley, J. Chem. Phys. **119**, 4833 (2003).
[3] A. Detken, E. Hardy, M. Ernst, and B. Meier, Chem. Phys. Lett. **356**, 298 (2002).
[4] M. Carravetta, M. Edén, X. Zhao, A. Brinkmann, and M. Levitt, Chem. Phys. Lett. **321**, 205 (2000).
[5] K. Riedel, J. Leppert, O. Ohlenschläger, M. Görlach, and R. Ramachandran, Chem. Phys. Lett. **395**, 356 (2004).
[6] M. Lee and W. I. Goldburg, Phys. Rev. **140**, A1261 (1965).
[7] M. Mehring and J. S. Waugh, Phys. Rev. B **5**, 3459 (1972).
[8] E. Vinogradov, P. Madhu, and S. Vega, Chem. Phys. Lett. **354**, 193 (2002).
[9] J. S. Waugh, L. M. Huber, and U. Haeberlen, Phys. Rev. Lett. **20**, 180 (1968).
[10] U. Haeberlen and J. S. Waugh, Phys. Rev. **175**, 453 (1968).
[11] P. Mansfield, J. Phys. C **4**, 1444 (1971).
[12] W.-K. Rhim, D. D. Elleman, and R. W. Vaughan, J. Chem. Phys. **59**, 3740 (1973).
[13] D. Burum and W.-K. Rhim, J. Chem. Phys. **71**, 944 (1979).
[14] D. Cory, J. Magn. Reson. **94**, 526 (1991).
[15] D. Sakellariou, A. Lesage, P. Hodgkinson, and L. Emsley, Chem. Phys. Lett. **319**, 253 (2000).
[16] B. Elena, G. de Paëpe, and L. Emsley, Chem. Phys. Lett. **398**, 532 (2004).
[17] A. Lesage, D. Sakellariou, S. Hediger, B. Elena, P. Charmont, and S. Steuernagel, J. Magn. Reson. **163**, 105 (2003).
[18] C. A. Michal, J. Chem. Phys. **118**, 3451 (2003).
[19] P. Eles and C. A. Michal, J. Chem. Phys. **121**, 10167 (2004).
[20] A. Bielecki, A. C. Kolbert, and M. H. Levitt, Chem. Phys. Lett. **155**, 341 (1989).
[21] E. Vinogradov, P. Madhu, and S. Vega, Chem. Phys. Lett. **314**, 443 (1999).
[22] E. Vinogradov, P. Madu, and S. Vega, J. Chem. Phys. **115**, 8983 (2001).
[23] L. Bosman, P. Madhu, S. Vega, and E. Vinogradov, J. Magn. Reson. **169**, 39 (2004).
[24] A. Abragam, *Principles of Nuclear Magnetism* (Oxford University Press, Oxford, 1961).
[25] F. Bloch and A. Siegert, Phys. Rev. **57**, 522 (1940).
[26] C. Michal, Rev. Sci. Instrum. **73**, 453 (2002).